




Inhibition of lipid kinase PIKfyve reveals a role for phosphatase Inpp4b in the regulation of PI(3)P-mediated lysosome dynamics through VPS34 activity

Received for publication, April 2, 2022, and in revised form, June 13, 2022. Published, Papers in Press, June 26, 2022.

<https://doi.org/10.1016/j.jbc.2022.102187>

Golam T. Saffi¹, Cheng An Wang¹, Emily M. Mangialardi¹, Jean Vacher² , Roberto J. Botelho³ , and Leonardo Salmena^{1,4,*} 

From the ¹Department of Pharmacology & Toxicology, University of Toronto, Toronto, Ontario, Canada; ²Institut de Recherches Cliniques de Montréal (IRCM), Département de Médecine, Université de Montréal, Montréal, Québec, Canada; ³Department of Chemistry and Biology, Ryerson University, Toronto, Ontario, Canada; ⁴Princess Margaret Cancer Centre, University Health Network, Toronto, Ontario, Canada

Edited by Alex Tokor

Lysosome membranes contain diverse phosphoinositide (PtdIns) lipids that coordinate lysosome function and dynamics. The PtdIns repertoire on lysosomes is tightly regulated by the actions of diverse PtdIns kinases and phosphatases; however, specific roles for PtdIns in lysosomal functions and dynamics are currently unclear and require further investigation. It was previously shown that PIKfyve, a lipid kinase that synthesizes PtdIns(3,5)P₂ from PtdIns(3)P, controls lysosome “fusion-fission” cycle dynamics, autophagosome turnover, and endocytic cargo delivery. Furthermore, INPP4B, a PtdIns 4-phosphatase that hydrolyzes PtdIns(3,4)P₂ to form PtdIns(3)P, is emerging as a cancer-associated protein with roles in lysosomal biogenesis and other lysosomal functions. Here, we investigated the consequences of disrupting PIKfyve function in *Inpp4b*-deficient mouse embryonic fibroblasts. Through confocal fluorescence imaging, we observed the formation of massively enlarged lysosomes, accompanied by exacerbated reduction of endocytic trafficking, disrupted lysosome fusion-fission dynamics, and inhibition of autophagy. Finally, HPLC scintillation quantification of ³H-*myo*-inositol labeled PtdIns and PtdIns immunofluorescence staining, we observed that lysosomal PtdIns(3)P levels were significantly elevated in *Inpp4b*-deficient cells due to the hyperactivation of phosphatidylinositol 3-kinase catalytic subunit VPS34 enzymatic activity. In conclusion, our study identifies a novel signaling axis that maintains normal lysosomal homeostasis and dynamics, which includes the catalytic functions of *Inpp4b*, PIKfyve, and VPS34.

Lysosomes are membrane-bound organelles that serve as a cell's main degradative center (1, 2). Lysosomes are also key sentinels of cellular nutrient concentration and metabolic activity and have a critical role in initiating diverse signal transduction pathways (3–5). Lysosomal membranes include diverse phosphoinositides (PtdIns), known to control lysosome function, trafficking, permeability, and general homeostasis

through their ability to coordinate recruitment of critical proteins (6). PtdIns exist in seven different forms which are defined by the phosphorylation status of the 3, 4, and/or 5 hydroxyl groups of their inositol head, a process controlled by a number of cellular kinases and phosphatases with PtdIns specificity (7, 8).

Of notable importance on lysosomal membranes is phosphatidylinositol-3,5-bisphosphate [PtdIns(3,5)P₂], generated through 5'-phosphorylation of phosphatidylinositol-3-monophosphate [PtdIns(3)P] by Phosphoinositide Kinase, FYVE-Type Zinc Finger Containing (PIKfyve) (9, 10). Pharmacological or genetic inhibition of PIKfyve and subsequent depletion of PtdIns(3,5)P₂ has been demonstrated to disrupt lysosomal-related processes including autophagic flux, endocytic and phagocytic cargo delivery to lysosomes, substrate export from lysosome, and calcium release (11–14). Notably, inhibition of PIKfyve also leads to a dramatic enlargement of lysosomes, a phenomenon explained in part by defective membrane recycling from endosomes and/or lysosomes (9, 15). PtdIns(3,5)P₂ depletion and lysosome enlargement in various cell lines can be effectively induced by the pharmacological PIKfyve inhibitor apilimod (16, 17). Specifically, apilimod interacts with the amino acid asparagine (N1939) predicted to be located within the ATP-binding pocket of the catalytic kinase domain of PIKfyve (18). More recently, Choy *et al.* attributed apilimod-induced lysosome enlargement to the disruption of lysosome fusion-fission cycling and/or disruption of “kiss-and-run”, a term which describes a transient membrane fusion event followed by rapid fission event that permits content exchange between lysosomes (11, 17, 19, 20). In their model, PIKfyve inhibition compromises lysosomal fission (the “run” event) and thus promotes lysosome coalescence which results in increased individual lysosome volume and reduced lysosome numbers (17, 21).

Emerging evidence suggests that other PtdIns including PtdIns(3)P, PtdIns(4)P, and PtdIns(3,4)P₂ may also play important roles in regulating lysosomal homeostasis. For instance, PtdIns(3)P has been implicated in regulating lysosomal positioning and lysosomal mTORC1 activity (22).

* For correspondence: Leonardo Salmena, leonardo.salmena@utoronto.ca.

VPS34, a class III PtdIns 3-kinase, is recruited by active GTP-bound Rab5 and Rab7 in complex with VPS15, toward early and late endosomes. VPS34-induced PtdIns(3)P generation regulates early and late endosomal morphology (23), intraluminal vesicle formation within late endosomes (24), and endosomal assembly of cargo recycling complex (24). Additionally, mTOR regulation of VPS34 activity controls lysosome tubular morphology (25). PtdIns(4)P has demonstrated important functions in lysosomal membrane fusion in late endocytic trafficking (26). PtdIns(3,4)P₂ was also demonstrated to promote repression of mTORC1 activity and cell growth through functions on lysosomal membranes (27). Notably, an emerging role for Inositol polyphosphate 4-phosphatase type II (INPP4B), a PtdIns phosphatase that dephosphorylates PtdIns(3,4)P₂ to form PtdIns(3)P, in lysosome homeostasis has been reported in diverse cancer settings (28, 29). Overexpression of INPP4B leads to depleted intracellular PtdIns(3,4)P₂ and promoted endosomal trafficking of cargo toward lysosomes in breast cancer (28), and our recent study implicates INPP4B in lysosomal biogenesis in leukemia cells (29). Overall, roles for PtdIns(3,4)P₂ and PtdIns(3)P in lysosomal function and dynamics are currently unclear and require further investigation.

To better understand a role for INPP4B in lysosome homeostasis, we investigated the consequences of PIKfyve inhibition in *Inpp4b*^{+/+} and *Inpp4b*^{-/-} mouse embryonic fibroblasts (MEFs). Surprisingly, PIKfyve inhibition with apilimod in *Inpp4b*^{-/-} fibroblasts leads to the formation of very massively enlarged lysosomes, compared to the typically enlarged lysosomes produced in *Inpp4b*^{+/+} fibroblasts. Our results suggest that exacerbated lysosomal enlargement was, at least in part, a result of aberrantly elevated levels of lysosomal PtdIns(3)P generated by increased activity of the Class III PtdIns 3-kinase VPS34 in *Inpp4b*^{-/-} cells. Together, these point to a novel role for *Inpp4b* in suppressing VPS34 activity and the existence of coordinated functions for *Inpp4b*, PIKfyve, and VPS34 in maintaining normal lysosomal homeostasis, dynamics, and function.

Results

PIKfyve inhibition in *Inpp4b*-null MEF leads to formation of massively enlarged LAMP1⁺ vacuoles

Treatment of *Inpp4b*^{+/+} and *Inpp4b*^{-/-} MEF with the specific PIKfyve inhibitor apilimod generated the formation of enlarged cellular vacuoles at 48 h of apilimod treatment in *Inpp4b*^{+/+} MEF by light microscopy; strikingly, *Inpp4b*^{-/-} MEF demonstrated an exacerbated vacuolation phenotype with many more massively enlarged vacuoles (Fig. 1A). Ectopic expression of the lysosomal specific membrane protein (LAMP1) tagged to mCherry (LAMP1-mCherry) followed by fluorescence microscopy revealed that nearly all the enlarged vacuoles in *Inpp4b*^{+/+} and *Inpp4b*^{-/-} MEF were membrane positive for LAMP1 indicating a lysosomal origin for enlarged vacuoles (Figs. 1B and S1A). Quantitation of LAMP1 immunofluorescence (IF) confirmed that enlarged vacuoles were average significantly larger and significantly more abundant in

apilimod-treated *Inpp4b*^{-/-} MEFs than in *Inpp4b*^{+/+} MEF (Fig. 1, C–E). Total LAMP1 staining demonstrated that vehicle-treated *Inpp4b*^{-/-} MEF had less lysosomal content compared to *Inpp4b*^{+/+} MEF (Fig. 1F). Apilimod treatment significantly increased total LAMP1 staining in both *Inpp4b*^{+/+} and *Inpp4b*^{-/-} MEF in a proportional manner, indicating that induction of lysosomal content was not compromised in *Inpp4b*^{-/-} MEF (Fig. 1, F, S1, E and F). These findings were corroborated with LysoTracker Red (LTR; Fig. S1, D–F) and ectopic expression of a LAMP1-mCherry in *Inpp4b*^{+/+} and *Inpp4b*^{-/-} MEF (Fig. S1, A–C).

To confirm that the aberrant vacuolation response upon apilimod treatment was indeed a result of *Inpp4b* deficiency, we transduced *Inpp4b*^{-/-} MEF with constructs that express *Inpp4b*-EGFP, catalytically dead *Inpp4b*^{C845A}-EGFP, and control EGFP and treated with apilimod or vehicle and measured vacuole size and number (Fig. S1, G–I). *Inpp4b*-EGFP expression in *Inpp4b*^{-/-} MEF generated significantly reduced numbers and average size of enlarged vacuoles upon apilimod treatment compared to non-transduced and EGFP negative controls (Fig. S1, G–I). Notably, transduction of *Inpp4b*^{C845A}-EGFP in *Inpp4b*^{-/-} MEF was unable to rescue the number and size of enlarged vacuoles upon apilimod treatment (Fig. S1, G–I). Exacerbated lysosomal enlargement observed with INPP4B deficiency was also generalizable to human cells, as determined in U2OS cells upon INPP4B knockdown with RNAi (Fig. S2, A–E). We also evaluated the effect of *Inpp4b* suppression on late endosomes. *Inpp4b*^{-/-} MEF displayed reduced CD63⁺ late endosome puncta number (Fig. S3). Notably, apilimod treatment did not alter CD63⁺ late endosome levels, indicating that late endosomes do not reflect the changes observed in lysosomal levels. This suggests that CD63⁺ late endosomes are not affected by apilimod, and that PIKfyve inhibition may selectively disrupt lysosomal homeostasis and dynamics (Fig. S3). Overall, apilimod treatment in *Inpp4b*^{-/-} MEF demonstrate an exacerbated lysosomal vacuolation phenotype compared to *Inpp4b*^{+/+} MEF that can be rescued by WT *Inpp4b*, but not a catalytically dead *Inpp4b*. These data suggest an important role for *Inpp4b* phosphatase function in maintaining lysosomal dynamics and homeostasis.

****Inpp4b* deficiency exacerbates apilimod-mediated inhibition of endocytic trafficking to lysosomes***

We attempted to measure lysosome dynamics using Lucifer yellow (LY), a membrane impermeable fluorescent dye that is internalized by endocytosis and accumulates within lysosomes. LY fluorescence provides an effective tool to specifically delineate lysosomes for accurate measurement of lysosome number and volume (30, 31). MEF were treated with vehicle or apilimod prior to LY pulses of 1, 2, and 4 h. Flow cytometry was used to measure LY uptake which demonstrated that apilimod elevated total intracellular LY-fluorescence similarly in both *Inpp4b*^{+/+} and *Inpp4b*^{-/-} MEF for up to 4 h (Fig. S4). To monitor specific LY trafficking to lysosomes, we labeled lysosomes with ectopic expression of LAMP1-mCherry and measured colocalization with LY (Fig. S5A). Apilimod treatment demonstrated a markedly reduced accumulation of LY to lysosomes in *Inpp4b*^{+/+} MEF.

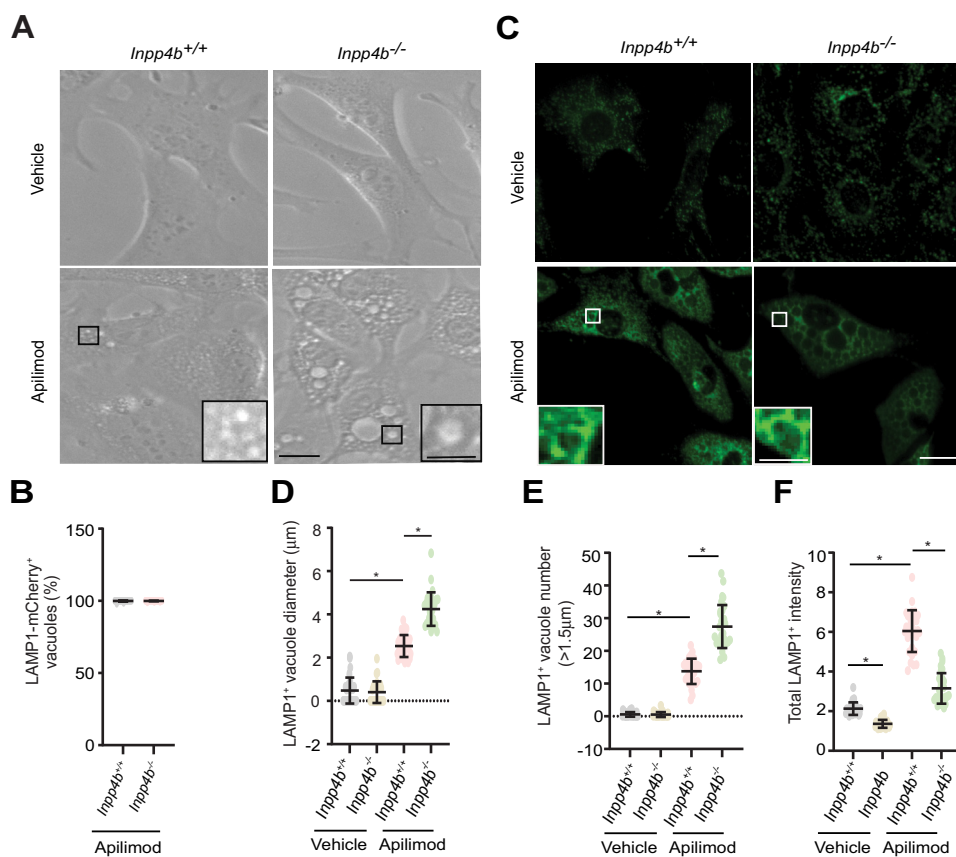


Figure 1. PIKfyve inhibition in *Inpp4b*-deficient cells leads to altered lysosome homeostasis. *A*, *Inpp4b*^{+/+} or *Inpp4b*^{-/-} MEF cells were incubated with vehicle or 10 nM apilimod for 48 h followed by imaging with DIC optics. *B*, scoring for percentage of LAMP1-mCherry membrane positive vacuoles formed upon apilimod treatment. *C*, fluorescence micrographs of LAMP1 immunostaining for *Inpp4b*^{+/+} or *Inpp4b*^{-/-} MEFs treated with vehicle or 10 nM apilimod for 48 h. *D*, mean vacuole diameter (µm) positive for LAMP1 membrane immunostain, (*E*) LAMP1 positive vacuole number (>1.5 µm in diameter) per cell across indicated treatments, and (*F*) LAMP1 puncta intensity. The scale bar represents 20 µm, zoomed inset: 5 µm. Data represent ± SD from three independent experiments with 25 to 30 cells assessed per treatment condition per experiment for (*B*–*F*). Statistical significance was measured by ANOVA and multiple Student's *t* test and represented as * (*p* < 0.05). INPP4B, inositol polyphosphate 4-phosphatase type II; MEF, mouse embryonic fibroblast; PIKfyve, Phosphoinositide Kinase, FYVE-Type Zinc Finger Containing.

Comparatively, *Inpp4b*^{-/-} MEF has significantly less LY accumulation at lysosomes compared to *Inpp4b*^{+/+} MEF for up to 2 h, indicating a slower colocalization of LY with lysosomes with *Inpp4b* deficiency (Fig. S5, *A* and *B*). We performed the same assay but replaced LY with DQ-BSA, bovine serum albumin labeled with a self-quenched BODIPY TR-X dye that upon lysosomal delivery is cleaved by lysosomal hydrolases, resulting in bright green fluorescent signal (32, 33). We observed that DQ-BSA activation was delayed but not inhibited in apilimod-treated *Inpp4b*^{-/-} MEF (Fig. S5C), suggesting that degradation of lysosomal cargo was not compromised. These findings indicate that PIKfyve inhibition reduces the ability of endocytosed cargo to reach terminal lysosomes, with no major effects on lysosomal proteolysis. Interestingly, like the vacuolation phenotype, apilimod-mediated accumulation was exacerbated in *Inpp4b*^{-/-} MEF, further indicating a role for *Inpp4b* in lysosomal trafficking (11, 34).

Inpp4b deficiency exacerbates apilimod-mediated lysosome fusion-fission dynamics

Given that apilimod blocks lysosomal accumulation of endocytic cargo such as LY, we adjusted our treatment

conditions so that MEF were first pulsed with LY followed by acute treatment with apilimod (Fig. 2A). In these experiments, quantitation of LY-labeled lysosomes revealed that individual basal lysosome size was similar in *Inpp4b*^{+/+} or *Inpp4b*^{-/-} MEF. Apilimod induced significant lysosomal enlargement compared to vehicle, and lysosome enlargement in *Inpp4b*^{-/-} MEF was significantly larger than *Inpp4b*^{+/+} MEF (Fig. 2, *A* and *B*). *Inpp4b*^{-/-} MEF have fewer total lysosomes than *Inpp4b*^{+/+} MEF; and apilimod treatment reduced lysosome numbers in both *Inpp4b*^{+/+} or *Inpp4b*^{-/-} MEF (Fig. 2, *A* and *C*). Notably, total lysosomal content as measured by total cellular LY accumulation was significantly lower in *Inpp4b*^{-/-} MEF and remained unchanged upon apilimod treatment (Fig. 2, *A* and *D*). These data conform to a model whereby apilimod treatment promotes lysosomal coalescence, which is manifested as increased individual lysosome volume and reduced total lysosome numbers (16, 17, 35). Notably, *Inpp4b* deficiency exacerbates apilimod-induced lysosomal enlargement, thus providing further evidence of a role for *Inpp4b* in lysosomal homeostasis and dynamics which is revealed upon apilimod treatment.

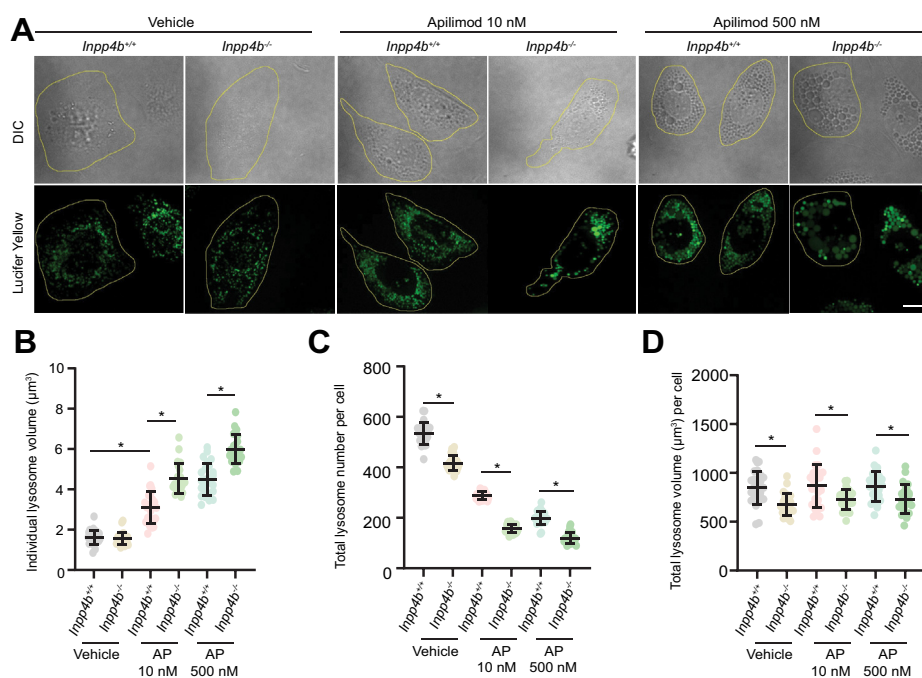


Figure 2. Lysosome volume and numbers are altered upon PIKfyve inhibition in *Inpp4b*-deficient cells. A, lysosomes of *Inpp4b*^{+/+} or *Inpp4b*^{-/-} MEFs prelabeled with Lucifer Yellow and exposed to vehicle or apilimod at indicated concentrations for 1 h. Fluorescence micrographs represent Z-projections of 25 to 30 Z-planes acquired through spinning disc confocal microscopy. Image analysis performed for individual lysosome volume (B), lysosome number per cell (C), and total lysosome volume per cell (D). The scale bar represents 25 μm. Data represent mean ± SD from three independent experiments, with 25 to 30 cells assessed per treatment condition per experiment. Statistical significance was measured by ANOVA and multiple Student's *t* test and represented as * (*p* < 0.05). INPP4B, inositol polyphosphate 4-phosphatase type II; MEF, mouse embryonic fibroblast; PIKfyve, Phosphoinositide Kinase, FYVE-Type Zinc Finger Containing.

Inhibition of lysosomal fission has been proposed as an explanation for apilimod-induced lysosome enlargement (16, 17, 35). To investigate the specific consequence of *Inpp4b* deficiency on “kiss-and-run” and/or “fusion-and-fission” cycles, live-imaging of LY-labeled lysosomes was recorded. *Inpp4b*^{+/+} and *Inpp4b*^{-/-} MEF treated with either vehicle or apilimod were monitored for up to 15 min and lysosomal fission events were recorded. Despite presenting similar fission rates in vehicle-treated *Inpp4b*^{+/+} and *Inpp4b*^{-/-} MEF, apilimod significantly reduced lysosome fission rates in *Inpp4b*^{+/+} MEF, and remarkably fission was nearly abrogated in *Inpp4b*^{-/-} MEF (Fig. 3, A and B and Movies S1–S4). This suggests that the enhanced lysosomal coalescence observed in *Inpp4b*^{-/-} MEF upon apilimod treatment is due to an exacerbated inhibition of lysosomal fission and *Inpp4b* deficiency alters lysosome dynamics such that they are sensitized to the lysosomal fission-inhibiting effects of apilimod.

Apilimod treatment induces differential effects on gene expression and lysosome function in *Inpp4b*^{+/+} and *Inpp4b*^{-/-} MEF

To shed light on the exacerbated vacuolation phenotypes observed with *Inpp4b* deficiency, we assessed the effects of apilimod treatment on lysosomal biogenesis in *Inpp4b*^{+/+} and *Inpp4b*^{-/-} MEF. Firstly, evaluation of nuclear translocation of Transcription Factor EB (TFEB) (36), a key regulator of lysosomal gene transcription that undergoes nuclear translocation upon apilimod treatment, did not reveal any difference

between *Inpp4b*^{+/+} and *Inpp4b*^{-/-} MEF (Fig. 4, A and B). Next, transcript levels of representative lysosomal genes including *LAMP1*, *MCOLN1*, *CTSB*, *CTSD*, *ATP6V1D*, and *ATP6V1H* were measured by TaqMan qPCR after vehicle or apilimod treatment. In vehicle-treated cells, *Inpp4b*^{-/-} MEF demonstrated modest, but significantly reduced expression of all lysosomal genes, except for *CTSD* (Fig. 4C). Strikingly, apilimod treatment led to a ~3-fold increase of all lysosomal transcripts tested in *Inpp4b*^{-/-} MEF, whereas *Inpp4b*^{+/+} MEF showed no significant changes under the same conditions (Fig. 4C). Immunoblotting of representative lysosomal proteins demonstrated that *Inpp4b*^{-/-} MEF have reduced steady state expression of LAMP1, pre- and mature-cathepsin B, and V-ATPase V1H, similar to transcript expression profiles (Fig. 4, D and E). However, apilimod treatment of *Inpp4b*^{+/+} MEF demonstrated elevated levels of the lysosomal membrane-bound LAMP1 and V-ATPase V1H proteins, but no significant change in cathepsin proteins. By contrast, apilimod treatment demonstrated significantly elevated expression of all lysosomal proteins tested in *Inpp4b*^{-/-} MEF (Fig. 4, D and E). To quantify the differential effects of apilimod on lysosomal proteolytic function, we used the membrane permeable cathepsin B substrate-Magic Red which upon hydrolysis forms membrane impermeable fluorescent cresyl-violet and accumulates within functional lysosomes (37). The results of this assay paralleled the transcript and protein expression levels of cathepsin B, where apilimod treatment had no effect in *Inpp4b*^{+/+} MEF, and in *Inpp4b*^{-/-} MEF, despite having a reduced steady state cathepsin B activity, apilimod treatment

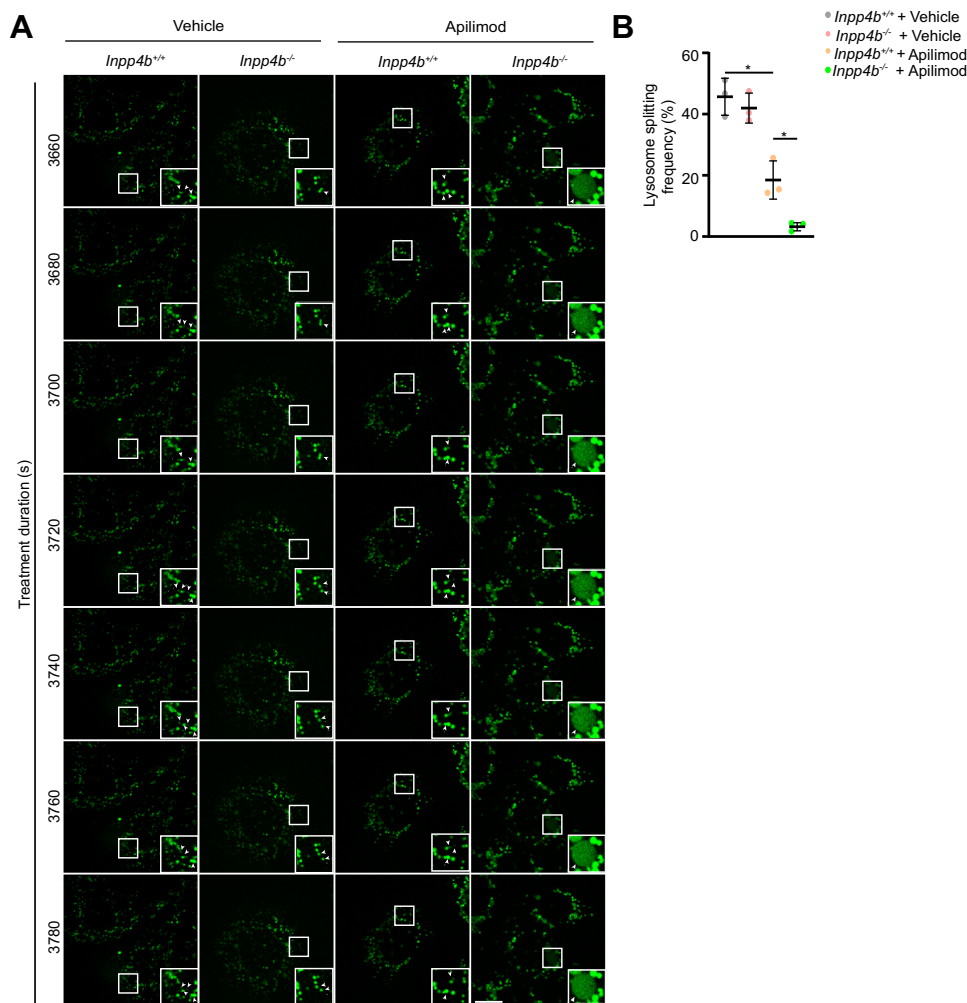


Figure 3. Lysosome “kiss-and-run” dynamics are disrupted upon PIKfyve inhibition in *Inpp4b*-deficient cells. *A*, *Inpp4b*^{+/+} or *Inpp4b*^{-/-} MEFs were prelabeled with Lucifer Yellow followed by treatment with vehicle or 10 nM apilimod. Time in sec (s) refers to time post treatment. See [Movies S1–S4](#) for full capture imaging videos. Inset represents an enlarged section from the field of view tracking individual lysosome particle dynamics over time. The scale bar represents 20 μ m, zoomed inset: 10 μ m. *B*, lysosome splitting frequency over 15 min for WT or Null MEFs treated with vehicle or apilimod demonstrate reduced splitting in PIKfyve inhibited WT MEFs and to a greater extent in PIKfyve inhibited Null MEFs, indicative of possible reduced lysosome fission. Data represent mean \pm SD from three independent experiments, where at least a total of 1300 lysosomes were tracked for 1 to 3 cells over 15 min. Statistical significance was measured by ANOVA and multiple Student’s *t* test and represented as * ($p < 0.05$). INPP4B, inositol polyphosphate 4-phosphatase type II; MEF, mouse embryonic fibroblast; PIKfyve, Phosphoinositide Kinase, FYVE-Type Zinc Finger Containing.

led to a more than 3-fold induction of cathepsin B activity (Fig. 4, *F* and *G*). Although activation of nuclear translocation of TFEB by apilimod was no different in *Inpp4b*^{+/+} and *Inpp4b*^{-/-} MEF, lysosomal gene expression, protein expression, and proteolytic function of lysosomes are differentially impacted by apilimod treatment in *Inpp4b*^{+/+} and *Inpp4b*^{-/-} MEF.

Inhibition of autophagy by apilimod is potentiated in *Inpp4b*-deficient cells

PIKfyve inhibition has been demonstrated to inhibit autophagy in various physiological and pathological settings upon extended PIKfyve inhibition, but not upon acute exposure (12, 16, 38). We evaluated how apilimod treatment affected autophagy in the context of *Inpp4b* deficiency by first measuring levels of MAP1LC3A/B (LC3), a membrane protein specifically expressed on autophagosomes by IF with anti-LC3 antibodies

(39). Total cellular LC3 staining was similar in vehicle-treated MEF. Apilimod treatment induced LC3 levels to significantly higher levels in *Inpp4b*^{-/-} MEF than in *Inpp4b*^{+/+} MEF (Fig. 5, *A* and *B*). Notably, the corresponding elevation in autophagosome levels induced by apilimod in *Inpp4b*^{-/-} MEF was fully rescued by ectopic INPP4B expression, indicating that LC3 induction levels are restricted by *Inpp4b* (Fig. S6, *A–C*). We also assessed extent of autolysosome formation by quantitating colocalization LAMP1-mCherry fluorescence and LC-3 by IF. Relative to vehicle-treated MEF, colocalization of LAMP1 (lysosomes) and LC3 (autophagosomes) was elevated upon apilimod treatment, and *Inpp4b*^{-/-} MEF had significantly higher levels of colocalization than *Inpp4b*^{+/+} MEF (Fig. 5, *A* and *C*). Autophagy was also assessed by measuring LC-3 status by immunoblotting (40). During autophagy, cytosolic LC3-I (~16 kDa) is conjugated with phosphatidylethanolamine on the phagophore membrane to form LC3-II (~14 kDa). LC3-II is absent in vehicle-treated *Inpp4b*^{+/+} and *Inpp4b*^{-/-} MEF

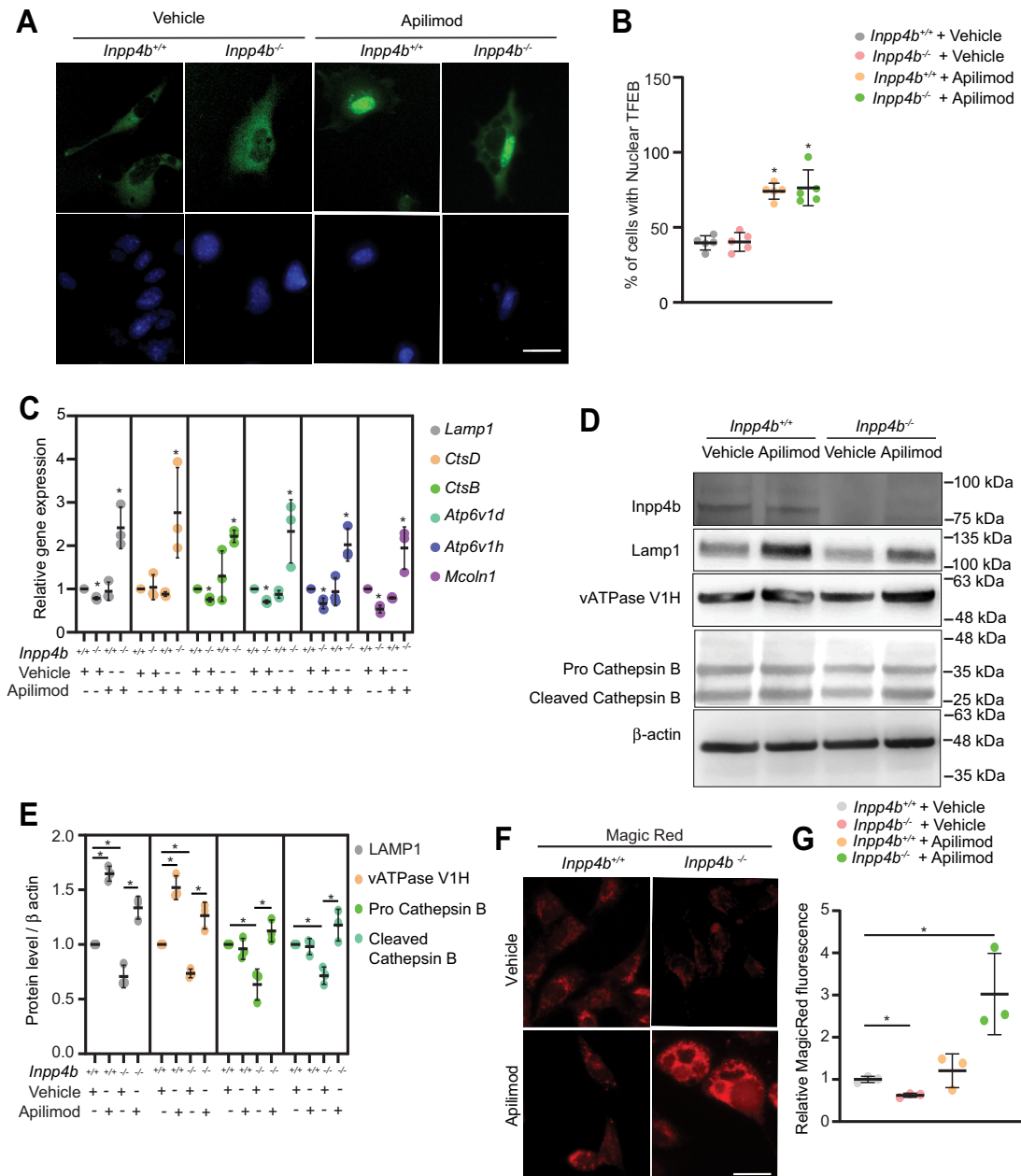


Figure 4. PIKfyve inhibition in *Inpp4b*-deficient cells disrupts lysosome gene expression. *A*, *Inpp4b*^{+/+} or *Inpp4b*^{-/-} MEFs transiently expressing pEGFP-TFEB and treated with vehicle or apilimod 10 nM for 48 h. DNA was stained with Hoechst 33342. *B*, TFEB nuclear translocation measured as percentage of cells demonstrating nuclear EGFP-TFEB for (*A*). The scale bar represents 25 μm. *C*, *Inpp4b*^{+/+} or *Inpp4b*^{-/-} MEFs treated with vehicle or apilimod 10 nM for 48 h followed by qRT-PCR analysis of lysosome gene expression normalized against Actb. Shown is mean ± SD from three independent experiments. *D*, immunoblot of *Inpp4b*^{+/+} or *Inpp4b*^{-/-} MEFs treated with vehicle or apilimod 10 nM for 48 h followed by assessment of select lysosomal proteins as indicated. *E*, analysis of protein levels from (*D*) shown as mean ± SD from three independent experiments. Data represent ± SD from five independent experiments with 30 to 35 cells assessed per treatment condition per experiment for (*A* and *B*). *F*, *Inpp4b*^{+/+} or *Inpp4b*^{-/-} MEF treated with vehicle or apilimod 10 nM for 48 h followed by Magic red incubation for 1 h. The scale bar represents 25 μm. *G*, quantification of Magic red intensity from (*F*) as measured through flow cytometry and mean ± SD from three independent experiments. Statistical significance was measured by ANOVA and multiple Student's *t* test and represented as * (*p* < 0.05). INPP4B, inositol polyphosphate 4-phosphatase type II; MEF, mouse embryonic fibroblast; PIKfyve, Phosphoinositide Kinase, FYVE-Type Zinc Finger Containing; TFEB, Transcription Factor EB.

(Figs. 5, *D* and *E* and *S7*), however apilimod treatment significantly induced LC3-II levels in *Inpp4b*^{+/+} MEF, and even further induction was observed in *Inpp4b*^{-/-} MEF (Figs. 5, *D* and *E* and *S7*). Similar observations were made in U2OS cells where INPP4B expression was silenced with siRNA (Fig. *S2E*).

Autophagy was further assessed by estimating autophagic flux using a reporter system which expresses a fusion of LC3 protein with the acid-insensitive mCherry protein and the

acid-sensitive GFP protein (41, 42). This reporter permits the estimation of autophagic flux—autophagosome to autolysosome transition—by measuring the ratio of yellow (mCherry⁺ GFP⁺) or red (mCherry⁺ GFP⁻) puncta, respectively (12, 43, 44). In vehicle-treated *Inpp4b*^{+/+} and *Inpp4b*^{-/-} MEF, we observed predominantly red fluorescence indicating functional transition through autophagy (Fig. 5, *F* and *G*). By contrast, apilimod treatment resulted in predominantly yellow puncta in

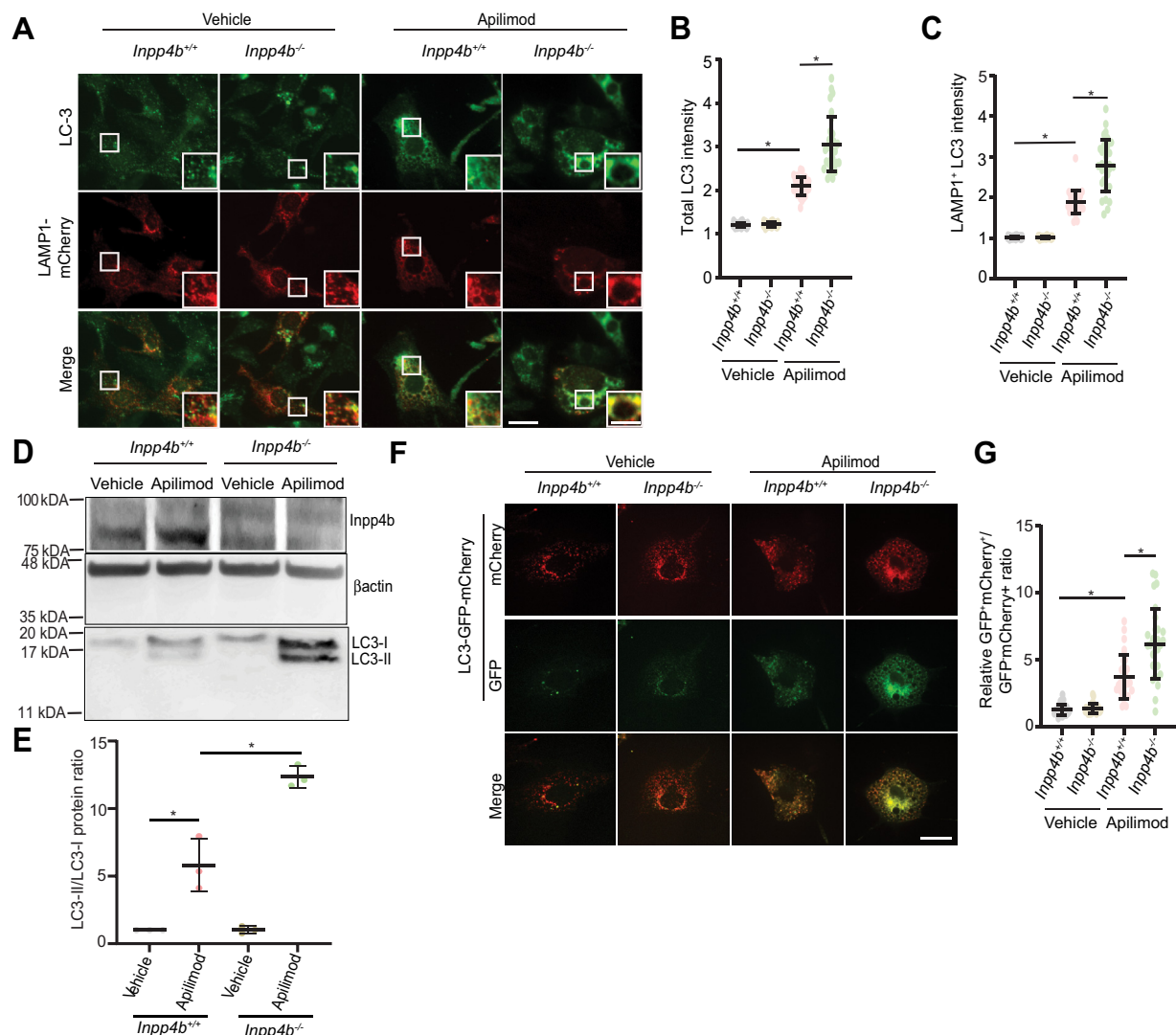


Figure 5. Autophagic flux is blocked upon PIKfyve inhibition in *Inpp4b*-deficient cells. *A*, *Inpp4b*^{+/+} or *Inpp4b*^{-/-} MEFs transiently expressing LAMP1-mCherry to mark lysosomes and treated with vehicle or apilimod 10 nM for 48 h, followed by immunostain against LC3. *B*, quantifications of LC3 puncta intensity per cell across indicated conditions to measure autophagosome levels and (*C*) LC3 intensity overlapping on LAMP1-positive lysosomes where increased LC3/LAMP1 intensity ratio indicate autolysosome formation. *D*, immunoblot of *Inpp4b*^{+/+} or *Inpp4b*^{-/-} MEFs treated with vehicle or apilimod 10 nM for 48 h and assessed for protein levels of *Inpp4b*, LC3, and Beta actin as loading control. *E*, quantification of immunoblot from (*D*) for LC3-II/LC3-I protein ratio shown as mean \pm SD from three independent experiments. *F*, *Inpp4b*^{+/+} or *Inpp4b*^{-/-} MEF transiently expressing *mCherry-EGFP-LC3B* and treated with vehicle or apilimod 10 nM for 48 h. *G*, quantification of LC-3 green puncta over red puncta intensity ratio. The scale bar represents 15 μ m, zoomed inset: 5 μ m. Data represent mean \pm SD from three independent experiments, with 25 to 30 cells assessed per treatment condition per experiment for (*A*–*C*) and (*F*–*G*). Statistical significance was measured by ANOVA and multiple Student's *t* test and represented as * ($p < 0.05$). PIKfyve, Phosphoinositide Kinase, FYVE-Type Zinc Finger Containing; INPP4B, inositol polyphosphate 4-phosphatase type II; MEF, mouse embryonic fibroblast.

Inpp4b^{+/+} MEF and an even higher ratio of yellow to red puncta in *Inpp4b*^{-/-} MEF. (Fig. 5, *F* and *G*). Notably, the accumulation of yellow fluorescence (mCherry⁺ GFP⁺) in apilimod-treated *Inpp4b*^{-/-} MEF appear to be on the membranes of enlarged vacuoles. These data demonstrate that *Inpp4b* deficiency alone does not alter autophagic flux, however, apilimod treatment reveals that *Inpp4b* regulates autophagic flux in some conditions, including PIKfyve inhibition.

Inpp4b deficiency exacerbates apilimod-mediated PtdIns(3)P generation

Given the direct roles for PIKfyve and *Inpp4b* on PtdIns metabolism, we assessed how PtdIns homeostasis may be differentially affected in *Inpp4b*^{+/+} and *Inpp4b*^{-/-} MEF in

response to apilimod. We first measured total cell levels of PtdIns(3)P and PtdIns(3,5)P₂ through ³H-*myo*-inositol labeling and HPLC scintillation and quantification (40). *Inpp4b* deficiency did not alter PtdIns(3,5)P₂ levels, but as expected, apilimod treatment significantly reduced PtdIns(3,5)P₂ levels in both *Inpp4b*^{+/+} and *Inpp4b*^{-/-} MEF (Fig. 6A).

Total steady state PtdIns(3)P levels were also similar in *Inpp4b*^{-/-} MEF compared to *Inpp4b*^{+/+} MEF; this was unexpected given that PtdIns(3)P is the product of *Inpp4b* catalysis. Furthermore, apilimod treatment induced a significant \sim 1.3 fold increase of PtdIns(3)P in *Inpp4b*^{+/+} MEF and a \sim 3 fold increase of PtdIns(3)P in *Inpp4b*^{-/-} MEFs (Fig. 6A). To support these surprising findings, we also measured PtdIns(3)P by IF with an anti-PtdIns(3)P antibody in cells where lysosomes were

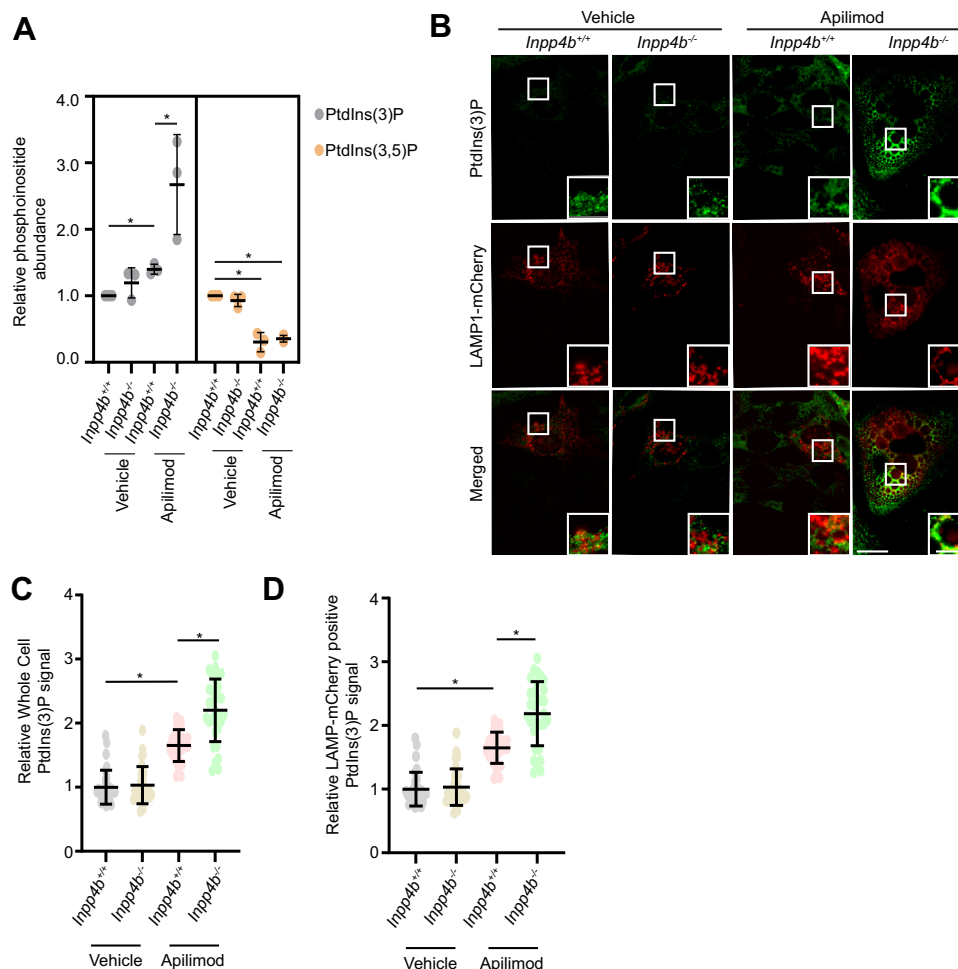


Figure 6. PIKfyve inhibition in *Inpp4b*-deficient cells leads to elevated PtdIns(3)P levels. A, ³H-myio-inositol incorporation and HPLC scintillation quantification of PtdIns(3)P and PtdIns(3,5)P₂ for *Inpp4b*^{+/+} or *Inpp4b*^{-/-} MEFs treated with vehicle or apilimod (n = 3). B, *Inpp4b*^{+/+} or *Inpp4b*^{-/-} MEFs transiently expressing LAMP1-mCherry and treated with vehicle or apilimod 10 nM for 48 h. C, total cell PtdIns(3)P or (D) LAMP1-mCherry positive PtdIns(3)P within a cell. The scale bar represents 20 μ m, zoomed inset: 5 μ m. Data represent \pm SD from three independent experiments with 25 to 30 cells assessed per treatment condition per experiment for (B–D). Statistical significance was measured by ANOVA and multiple Student's *t* test and represented as * (*p* < 0.05). INPP4B, inositol polyphosphate 4-phosphatase type II; MEF, mouse embryonic fibroblast; PtdIns, phosphoinositide; PtdIns(3,5)P₂, phosphatidylinositol-3,5-bisphosphate; PtdIns(3)P, phosphatidylinositol-3-monophosphate; PIKfyve, Phosphoinositide Kinase, FYVE-Type Zinc Finger Containing.

simultaneously marked with LAMP1-mCherry (Fig. 6B). Firstly, IF confirmed the elevated levels of total cellular PtdIns(3)P observed in apilimod-treated *Inpp4b*^{+/+} and *Inpp4b*^{-/-} MEF (Fig. 6C). Colocalization of PtdIns(3)P with LAMP1-mCherry revealed a similar pattern of PtdIns(3)P levels on lysosomal membranes (Fig. 6D). IF of PtdIns(3,4)P₂ revealed greater total and lysosomal levels of PtdIns(3,4)P₂, as expected in *Inpp4b*-deficient MEF (Fig. S8, A–C). Apilimod treatment had no effect on total cell or LAMP1-mCherry positive PtdIns(3,4)P₂ levels in *Inpp4b*^{+/+} MEF, however, there was a small but significant reduction in PtdIns(3,4)P₂ levels compared to steady state levels for *Inpp4b*^{-/-} MEF (Fig. S8, A–C). In sum, apilimod treatment led to a significant increase in total and lysosomal PtdIns(3)P in *Inpp4b*^{-/-} MEF, indicating an unexpected role for *Inpp4b* in suppressing cellular levels of PtdIns(3)P.

Apilimod-mediated lysosome enlargement is driven by VPS34-mediated PtdIns(3)P production

We sought to gain a further understanding of the mechanisms leading to elevated cellular PtdIns(3)P and its role in the

exacerbated lysosomal enlargement upon apilimod treatment in *Inpp4b*^{-/-} MEF. Given its major role in cellular PtdIns(3)P generation, we explored VPS34 functions (45). No changes in VPS34 protein levels were observed by immunoblot in *Inpp4b* deficiency nor in vehicle- or apilimod-treated conditions (Fig. 7A). Surprisingly, measurement of the lipid kinase activity of VPS34 demonstrated a significant elevation only in apilimod-treated *Inpp4b*^{-/-} MEF (Fig. 7B), thereby explaining elevated PtdIns(3)P levels.

To elucidate a role for PtdIns(3)P in the formation of massively enlarged vacuoles in apilimod-treated *Inpp4b*^{-/-} MEF, we reasoned that depletion of cellular PtdIns(3)P could attenuate this phenotype. Thus, we treated MEF with both apilimod and the specific VPS34 inhibitor, VPS34-IN1 (25, 46). PtdIns(3)P IF performed on VPS34-IN1-treated MEF demonstrated that VPS34 inhibition can effectively diminish total cellular and lysosomal localized PtdIns(3)P levels (Fig. 7, C–E). Notably, VPS34 inhibition in apilimod-treated *Inpp4b*^{-/-} MEF rescued the exacerbated lysosome enlargement but only to levels of enlargement normally observed in *Inpp4b*^{+/+} MEF;

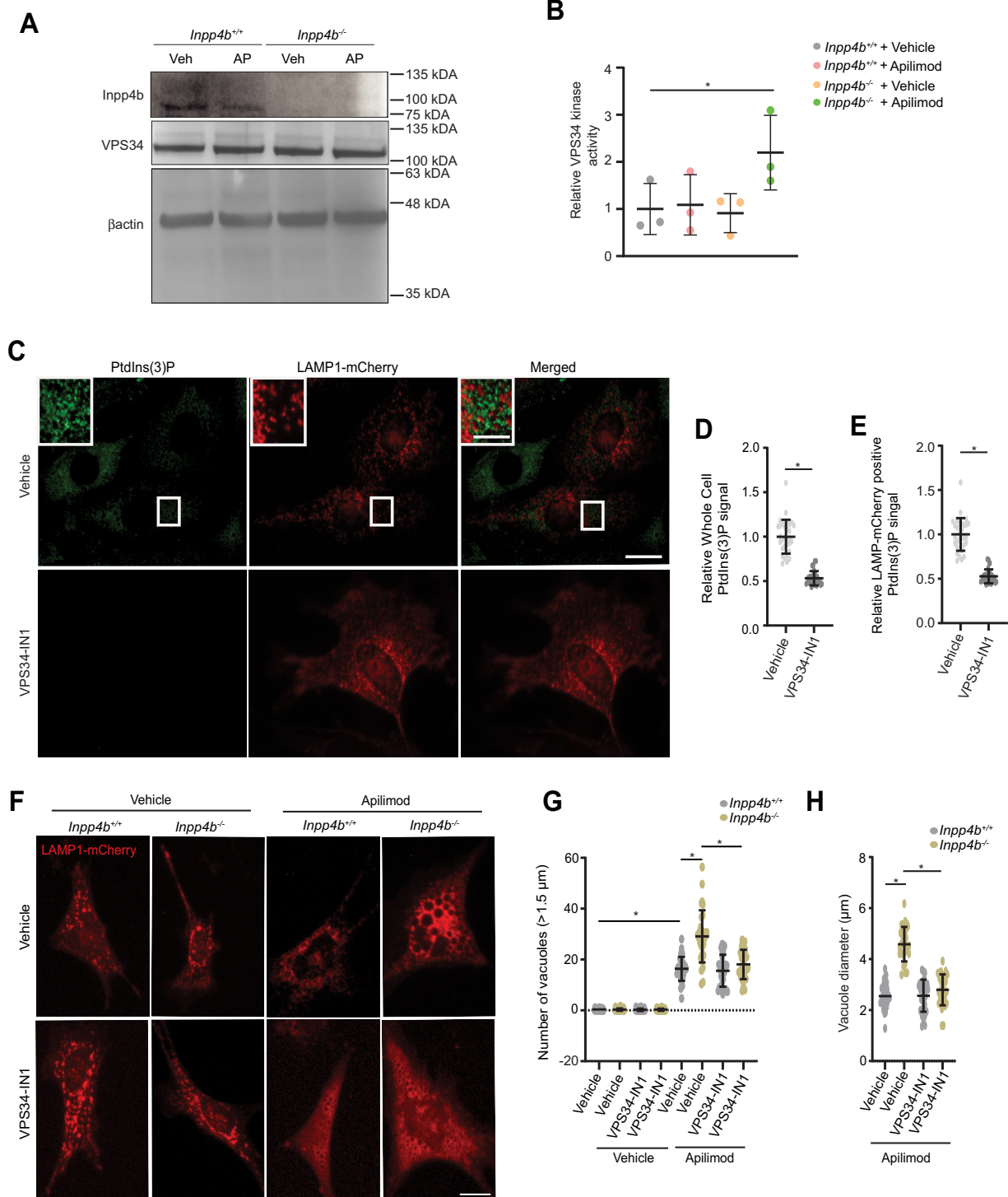


Figure 7. VPS34 activity is elevated upon PIKfyve inhibition in *Inpp4b*-deficient cells. *A*, *Inpp4b*^{+/+} or *Inpp4b*^{-/-} MEFs treated with vehicle or apilimod 10 nM for 48 h, followed by immunoblotting against *Inpp4b*, VPS34, or Beta Actin. *B*, *Inpp4b*^{+/+} or *Inpp4b*^{-/-} MEFs treated with vehicle or apilimod 10 nM for 48 h, followed by VPS34 immunoprecipitation and kinase assay to monitor VPS34 activity. *C*, *Inpp4b*^{+/+} MEF transiently expressing LAMP1-mCherry and treated with vehicle or 500 nM VPS34-IN1 for 48 h followed by PtdIns(3)P immunostain. *D*, quantification from (*C*) of total cell PtdIns(3)P fluorescence signal or (*E*) PtdIns(3)P fluorescence signal overlaid on LAMP1-mCherry positive regions within a cell. The scale bar represents 20 μm, zoomed inset: 5 μm. *F*, *Inpp4b*^{+/+} or *Inpp4b*^{-/-} MEF transiently expressing LAMP1-mCherry and treated with vehicle or apilimod 10 nM or VPS34-IN1 500 nM at various combinations for 48 h. *G*, quantification of LAMP1-positive vacuoles greater than 1.5 μm in diameter per cell and (*H*) mean vacuole diameter (μm). The scale bar represents 20 μm. Data represent ± SD from three independent experiments with 25 to 30 cells assessed per treatment condition per experiment. Statistical significance was measured by ANOVA and multiple Student's *t* test and represented as * (*p* < 0.05). INPP4B, inositol polyphosphate 4-phosphatase type II; MEF, mouse embryonic fibroblast; PtdIns, phosphoinositide; PtdIns(3)P, phosphatidylinositol-3-monophosphate; PIKfyve, Phosphoinositide Kinase, FYVE-Type Zinc Finger Containing.

VPS34-IN1 had little effect on the enlarged lysosome size and number in apilimod-treated *Inpp4b*^{+/+} MEF, indicating that induction of PtdIns(3)P levels may not be necessary or sufficient for normal apilimod responses (Fig. 7, F–H). In sum, VPS34-IN1 revealed that aberrant hyperactivation of VPS34 in *Inpp4b*^{-/-} MEF treated with apilimod leads to exacerbated lysosomal enlargement. These findings suggest the existence of a role for *Inpp4b* in the regulation of VPS34 activation, and thereby PtdIns(3)P levels, in cells undergoing lysosomal stress induced by PIKfyve inhibition.

Discussion

Lysosomes, the primary catabolic organelles in the cell, play pivotal roles in many cellular processes including cell differentiation, plasma membrane repair, programmed cell death, nutrient sensing, and stress responses (47). Thus, exquisite control of lysosome homeostasis, including the dynamic mechanisms that control total lysosomal content, number, and size are critical to maintaining normal lysosomal and cellular functions. Emerging data indicates key roles for PtdIns in maintaining lysosomal homeostasis. In this study, we explored the dynamics of PIKfyve inhibition and resultant PtdIns(3,5)P₂ depletion, which leads to disruption of lysosomal “fusion-fission” cycles by compromising “fission”, thereby generating enlarged coalescent lysosomes (11, 16, 17). PIKfyve inhibition also disrupts endocytic cargo delivery, autophagosome formation, and autophagic flux, possibly a result of lysosome membrane perturbations where lysosomes fail to resolve from other lysosomes, late endosomes, and autophagosomes (11, 12). PIKfyve has been shown to functionally coordinate with the Class III PI3-Kinase VPS34 through its catalytic product PtdIns(3)P, which serves as a membrane localization target for PIKfyve, as well as a substrate precursor for PtdIns(3,5)P₂ synthesis (45). Together, the functions of PIKfyve and VPS34 recruit and regulate components of endosomal and lysosomal recycling (48). This PIKfyve-VPS34 crosstalk suggests the existence of other PIKfyve cross talks with other PtdIns-modifying enzymes.

Emerging studies present a role for the lipid-phosphatase INPP4B in the regulation of lysosome-associated functions. Our group has demonstrated that *INPP4B* expression in acute myeloid leukemia regulates lysosomal biogenesis and functions which are crucial for leukemia stem cell maintenance, differentiation, and chemoresistance (29). Another study demonstrated that INPP4B depletion in triple negative breast cancer resulted in delayed EGFR trafficking from early endosomes to late endosomes/lysosomes (49). A role for INPP4B in lysosomal functions is further supported by the observation that elevated expression of INPP4B in *PIK3CA*-mutant ER⁺ breast cancer cells induce formation of late endosomes and lysosomes, increase cargo trafficking toward lysosomes, and promote endosomal sequestration and lysosomal degradation of key signaling proteins (28). Together, these data support a role for INPP4B in the enhancement of function and cellular content of lysosomes. Indeed, this study further supports this notion as *Inpp4b*-deficient MEF consistently demonstrated

reduced total lysosomal content and lysosome numbers as measured by LAMP1 IF, lysotracker labeling, and lysosomal accumulation of LY (Figs. 1, 2 and S1). Furthermore, lysosomal transcript and protein expression levels were reduced in *Inpp4b*^{-/-} MEF, together suggesting a role for *Inpp4b* in promoting and/or maintaining lysosomal content by controlling biogenesis through transcriptional mechanisms (Fig. 4). Since INPP4B and PIKfyve both regulate lysosome function, we sought to shed light on putative interactions between these two enzymes.

Apilimod-mediated PIKfyve inhibition in MEF leads to formation of numerous enlarged translucent cytoplasmic vacuoles readily seen by light microscopy. In previous studies, 20 nM apilimod for 1 h in RAW macrophages led to rapid lysosome enlargement to a volume of ~10 μm³. HeLa or RPE cells required 100 to 200 nM apilimod to generate lysosome of 3 to 4 μm³ (16, 17). By comparison, apilimod treatment of *Inpp4b*^{+/+} MEF at 10 nM or 500 nM for 1 h dilated lysosome volume to 3 μm³ or 4.5 μm³, respectively. The key findings made in this study stem from the observations that apilimod treatment of *Inpp4b*^{-/-} MEF generate significantly larger cytoplasmic vacuoles than apilimod-treated *Inpp4b*^{+/+}. This observation was the first indication of a putative crosstalk between INPP4B and PIKfyve. To gain further insight into the exacerbated vacuolation phenotype in *Inpp4b*-deficient MEF, we first confirmed that enlarged vacuoles were of lysosomal origin as proposed by Choy et al. (17). Loading of MEF with LY prior to apilimod stimulation permitted effective lysosomal accumulation, which then enabled the clear visualization and quantitation of lysosomal features after apilimod treatment. LY labeling confirmed that lysosome size and number were affected to a greater degree in *Inpp4b*^{-/-} MEF by apilimod; and that apilimod inhibits lysosomal accumulation of cargo, a phenotype which was also exacerbated in *Inpp4b*^{-/-} MEF. Lysosome dynamics in *Inpp4b*^{-/-} MEF were exquisitely sensitized to apilimod, as demonstrated by the severely compromised lysosomal fission, relative to the moderately compromised fission rates observed in *Inpp4b*^{+/+} MEF.

In our attempts to further understand the underlying biology responsible for the exaggerated response to apilimod observed in *Inpp4b*^{-/-} MEF, we observed that the expression of representative lysosomal gene transcripts were either unchanged or decreased in *Inpp4b*^{+/+} MEF treated with apilimod. *Inpp4b*^{-/-} MEF on the other hand demonstrated a significant 2-3-fold increase in the expression of all lysosomal transcripts tested. Elevated lysosomal biogenesis observed in *Inpp4b*^{-/-} MEF was not explained by the nuclear localization of Tfeb; however, altered Tfeb transactivation activity by phosphorylation and acetylation by the action of factors including mTORC1, PKC, PKD, GSK3β, and phosphatases such as the Ca²⁺-dependent calcineurin cannot be formally excluded with our data (50–52). Analysis of lysosomal protein levels showed that lysosomal membrane-embedded proteins including Lamp1 and V-ATPase (V1H) subunit were significantly elevated in *Inpp4b*^{+/+} and *Inpp4b*^{-/-} MEF upon apilimod treatment. On the other hand, cathepsin-B protein levels and activity are elevated only in apilimod-treated *Inpp4b*^{-/-} MEF,

suggesting that the stability of some lysosomal proteins may also be differentially regulated in apilimod-treated *Inpp4b*^{+/+} and *Inpp4b*^{-/-} MEF. Disruption of autophagic flux, which blocks turnover of lysosomal proteins (12, 38) may explain elevation of some lysosomal proteins (LAMP1 and V-ATPase). Also, it is currently unclear if elevated cathepsin-B protein and activity result due to disrupted feedback regulation from apilimod effects. In sum, the specific consequences of *Inpp4b* deficiency combined with PIKfyve inhibition on gene expression require further study.

Our data also show that apilimod can elevate autophagosome levels and promote colocalization with lysosomes to form autolysosomes, however, autolysosome maturation appears to be inhibited as indicated by reduced autophagic flux. Interestingly, enlarged lysosomes in apilimod-treated cells are proteolytically competent as measured by Magic Red and DQ-BSA suggesting that altered lysosomal membrane composition may confer resistance to membrane degradation or other membrane-associated processes required for autolysosome maturation. Our observations are consistent with previous studies regarding the consequences of apilimod (12, 53–55), with the exception that *Inpp4b*^{-/-} MEF display exacerbated versions of this phenotype.

Finally, we measured intracellular PtdIns levels in apilimod-treated MEF. PtdIns(3)P levels were observed to be unchanged in vehicle-treated MEF, which suggests that other major mechanisms govern PtdIns(3)P levels, and *Inpp4b* may only be a minor contributor. As previously reported, apilimod leads to moderately elevated levels of PtdIns(3)P, which we also observed in *Inpp4b*^{+/+} MEF (56). Surprisingly, apilimod treatment in *Inpp4b*^{-/-} MEF led to a dramatic increase in both total cellular and lysosomal levels of PtdIns(3)P. This observation was deemed paradoxical given that *Inpp4b* deficiency should generate less PtdIns(3)P and suggests that *Inpp4b* may regulate PtdIns(3)P levels through an indirect mechanism. To explain elevated PtdIns(3)P, our tests revealed that VPS34 activity, but not protein levels, was elevated. Furthermore, VPS34-IN1, a specific inhibitor of VPS34, depleted PtdIns(3)P and reversed the exacerbated lysosomal enlargement observed with *Inpp4b* deficiency. These data point to a direct role for VPS34 in apilimod-mediated PtdIns(3)P induction (Fig. 8). Furthermore, our results highlight a novel regulatory signaling axis linking PIKfyve, VPS34, and *Inpp4b* functions.

In conclusion, our study demonstrates that *Inpp4b* deficiency sensitizes cells and lysosomes to the plethora of effects conferred by apilimod-mediated PIKfyve inhibition, the most obvious of which is significantly exacerbated lysosomal enlargement compared to *WT* cells, most likely due to blocked fission and thus, enhanced lysosome coalescence. Similar exacerbated consequences are observed for various other phenotypes associated with PIKfyve inhibition including disrupted autophagy and reduced cargo delivery to lysosomes (11–14). Finally, we have uncovered a novel role for *Inpp4b* in regulating the activation of VPS34 activity and induction of PtdIns(3)P levels, which was only revealed upon lysosomal stress activated by PIKfyve inhibition. This function is mediated through a novel PIKfyve–VPS34–*Inpp4b* regulatory signaling axis.

Experimental procedures

MEF preparation, cell culture conditions, transfections, drug treatment

Immortalized *Inpp4b*^{+/+} and *Inpp4b*^{-/-} MEF were generated as previously detailed (51). MEF and U2OS cells were maintained in Dulbecco's Modified Eagle's Medium (DMEM) supplemented with 10% Fetal Bovine Serum (FBS). MEF or U2OS cells were transiently transfected with *pTWIST-mCherry*, *pTWIST-Inpp4b-mCherry*, *mCherry-Lamp1*, *mCherry-EGFP-LC3B*, *pEGFP*, *GFP-Inpp4b*, *GFP-Inpp4b (C845A)*, and *pEGFP-TFEB*. U2OS cells were stably transfected with *mCherry-Lamp1* through selection with 200 µg/ml G418 for 10 days. Transfections of MEF and U2OS cells performed with Fugene HD (Promega) at 3:1 of DNA:Fugene ratio for 24 h followed by washing and supplementation with complete DMEM growth media. siRNA-mediated gene silencing for *INPP4B* in U2OS cells carried out using DharmaFECT1 Transfection reagent (GE Dharmacon). Briefly, 0.1 nmol of nontargeting or *Inpp4b* siRNA (GE Dharmacon) mixed with 2 µl of DharmaFECT1 Transfection reagent in DMEM media without FBS was added to U2OS cells for 24 h, followed by washing off the transfection mix with PBS and growth of cells for 48 h with treatment before imaging and Western blot. MEF and U2OS cells treated with apilimod or VPS34-IN1 (Selleck Chemicals) to inhibit PIKfyve or VPS34 functions respectively at doses and durations indicated.

Retroviral transduction

3.0×10^6 HEK 293T cells were grown in a 10 cm dish for 24 h followed by calcium phosphate transfection. Briefly, 10 µg of retroviral plasmid *pWZL hygro SV40 T-Large* was mixed with 5 µg of pCL-Eco retroviral packaging vector and 2M CaCl₂ to a final volume of 300 µl in sterile water. The transfection mix was supplemented with equal volume of 2× HEPES-buffered saline (140 mM NaCl, 1.5 mM Na₂HPO₄) followed by addition to the cells. Following 24 h post transfection, the media was changed and supplemented with complete DMEM growth media. Media was collected 48 h and 72 h post transfection. Virus-enriched media was filtered through a 0.45-micron filter, supplemented with 8 µg/ml protamine sulfate, and added to MEF cells grown in 10 cm dishes. Infections were repeated every 8 h and MEF cells were selected for 4 days with 75 µg/ml hygromycin B.

Lysosome labeling

MEF cell lysosomes were labeled with 1 mg/ml LY (Thermo Fisher Scientific) for 2 h in complete growth media at 37 °C and 5% CO₂, followed by washing in PBS and supplementation of complete media for 1 h. LTR (Thermo Fisher) was also used to label MEF cell lysosomes by incubation at 1 µM for 30 min in complete growth media. Magic Red (Abcam) was used to assess lysosomal cathepsin B activity in MEF cells by incubation for 1 h according to manufacturer instructions.

Immunofluorescence

Immunolabeling of cells following apilimod treatment was performed by fixation with 4% (v/v) paraformaldehyde for

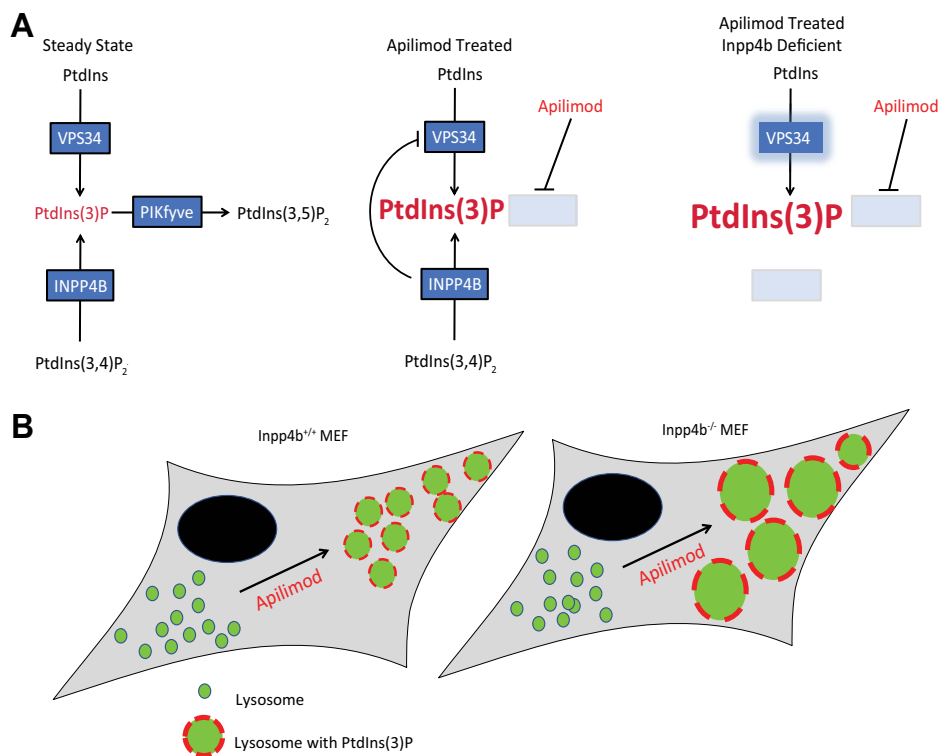


Figure 8. Model for lysosome enlargement upon PIKfyve inhibition in *Inpp4b* deficient cells. A, in the steady state, cycling of phosphoinositides involve VPS34-dependent conversion of phosphatidylinositol (PtdIns) to PtdIns(3)P, PtdIns(3,4)P₂ conversion by Inpp4b to PtdIns(3)P, and PtdIns(3)P conversion by PIKfyve to PtdIns(3,5)P₂. Apilimod-induced PIKfyve inhibition deplete PtdIns(3,5)P₂ to elevate the substrate PtdIns(3)P, and simultaneous PIKfyve and Inpp4b suppression further augment PtdIns(3)P levels. B, PIKfyve inhibition in *Inpp4b*^{+/+} MEF induce moderate lysosome enlargement, where lysosomes coalesce to become fewer in number and greater in individual lysosome volume. PIKfyve inhibition in *Inpp4b*^{-/-} MEF exacerbate lysosome enlargement, where lysosomes are much greater in individual volume and this enlargement is facilitated by enrichment of VPS34-induced membrane PtdIns(3)P. INPP4B, inositol polyphosphate 4-phosphatase type II; MEF, mouse embryonic fibroblast; PtdIns, phosphoinositide; PtdIns(3,5)P₂, phosphatidylinositol-3,5-bisphosphate; PtdIns(3)P, phosphatidylinositol-3-monophosphate; PIKfyve, Phosphoinositide Kinase, FYVE-Type Zinc Finger Containing.

15 min, permeabilization with 100% ice-cold methanol for 5 min, and blocking in 3% bovine serum albumin (v/v) in PBS. Cells were incubated with rabbit monoclonal antibody against mouse LC3B (1:200; Cell Signaling) and Alexa Fluor 488-conjugated goat polyclonal antibody against rabbit IgG (1:1000; Thermo Fisher). Alternatively, immunostaining was performed with rat monoclonal antibody against mouse LAMP1 (1:200, Clone 1D4B; Thermo Fisher) and Dylight 488-conjugated donkey polyclonal antibody against rat IgG (1:1000; Bethyl, Montgomery, TX). For CD63 immunostaining, fixations were performed with 4% (v/v) paraformaldehyde for 15 min, followed by permeabilization with 0.1% Triton X-100 for 10 min at room temperature. Immunostaining was performed with mouse monoclonal antibody against mouse CD63 (1:150; Novus Biologicals) and Dylight 488-conjugated Goat polyclonal antibody against mouse IgG (1:1000; Bethyl). Total cell PtdIns(3,4)P₂ or PtdIns(3)P immunostaining was performed by fixation with 4% (v/v) paraformaldehyde for 15 min, permeabilization with 20 μM digitonin (Promega) in buffer A (20 mM Pipes pH 6.8, 137 mM NaCl, 2.7 mM KCl) for 30 min, and blocking with buffer A containing 5% normal goat serum and 50 mM NH₄Cl. Immunostaining was performed with anti-PtdIns(3,4)P₂ IgG or anti-PtdIns(3)P IgG (Echelon) and Dylight 488-conjugated Goat polyclonal antibody against mouse IgG (1:1000; Bethyl). Samples are mounted onto microscope slides through DAKO fluorescent mounting media and imaged.

Live- and fixed-cell microscopy

Manual assessment of vacuole and lysosome size, number, LAMP1 positive vesicles, TFEB-GFP localization, Magic Red, or LTR-stained lysosomes were performed using EVOS-FL fluorescent inverted microscope controlled by EVOS XL core imaging system at 20× 0.4 NA. (Thermo Fisher) objective. Spinning disc confocal microscopy was used to perform live imaging through Olympus IX81 inverted microscope connected to Hamamatsu C9100-13 EMCCD camera with 60× 1.35 NA. objective and controlled by Volocity 6.3.0 (PerkinElmer). Time lapse live imaging performed with an environmental chamber set to 37 °C and 5% CO₂ in DMEM complete media. Fixed cells were observed through ZEISS AxioImager M2 Epifluorescence microscope connected to AxioCam MRm CCD camera and controlled by AxioVision Software Version 4.8 at 20× 0.8 NA. or 40× 1.4 NA. objective (Carl Zeiss).

Image analysis

To identify vacuoles as LAMP-1+ and of lysosomal origin, first, we set a minimum size threshold exclusion parameter to identify vacuoles as being greater than 1.5 μm in diameter on light microscopy using ImageJ. LAMP-1-mCherry fluorescence was then overlaid on these enlarged vacuoles and percentage LAMP-1-mCherry positivity was calculated. To

measure the percentage of cells with nuclear TFEB, cells were scored to have nuclear TFEB if the nucleus had greater intensity than cytosol using ImageJ. To measure the percentage of lysosomes filled with LY per cell, images imported into ImageJ and number of LAMP1-positive vesicles were manually scored for presence of LY signal within the lysosome lumen.

To quantify LAMP1 or LC3 immunostaining through ImageJ, intensity thresholding was applied to identify fluorescent structures and the mean intensity was obtained for each cell. To quantify LC3 intensity over LAMP1-positive structures, ImageJ was used to threshold for LAMP1-mCherry signal and generating a mask, which was applied to the green (LC3 immunostain) channel to measure LC3 intensity on LAMP1-mCherry positive regions. For MEF cells transiently expressing mCherry-eGFP-LC3B, similar approach was used to determine LC3 green puncta intensity over LC3 red puncta structures where relative intensity ratio greater than 1 indicate formation of autolysosomes due to reduced autophagic flux. Similar image analysis technique was applied for MEF cells transiently expressing LAMP1-mCherry to evaluate PtdIns(3,4)P₂ or PtdIns(3)P levels overlaid on LAMP1-mCherry positive regions within a cell. To quantify CD63 puncta number per cell, intensity thresholding was similarly applied to identify fluorescent puncta structures followed by total CD63 puncta number per cell.

To analyze lysosome-to-cytosol intensity ratio of INPP4B-mCherry, images were imported into ImageJ, and lines were assigned to nucleus-excluded areas of a cell measuring 40-pixel in length and 5-pixel in width. Intensity plot profiles were acquired and exported into excel spreadsheet. Intensity arranged according to values and ratio obtained for highest 10 pixels over lowest 10 pixels (F_H/F_L fluorescent ratio), where ratio values of approximately 1 represent cytosolic distribution.

To measure lysosome volume and number per cell, particle detection and volumetric tools from Volocity 6.3.0 were used. Briefly, Z-stack images imported into Volocity and punctate lysosome structures identified by applying a 2× cytosol intensity threshold to exclude cytosol and background. Further criteria to include particles greater than 0.3 μm^3 removed noise-derived particles. Each cell was isolated by drawing region interest for individual cell analysis. Quantification of lysosome splitting frequency was performed through Imaris (BitPlane) using 'ImarisTrackLineage' module, where lysosome splitting was defined as frequency of events where two particles were produced from a single particle.

VPS34 immunoprecipitation and VPS34 kinase assay

Following vehicle or apilimod treatment of *Inpp4b*^{+/+} and *Inpp4b*^{-/-} MEF cells, VPS34 immunoprecipitation was performed using the protocol from Cell Signaling (#4263 from Cell Signaling). Five hundred microgram of total protein lysate was incubated with VPS34 antibody #4263 (1:50) overnight at 4 °C. Precleared protein A magnetic beads (Cell Signaling) was incubated with immunocomplex for 20 min at room temperature on a shaking rotator. The magnetic beads were washed five times with TBST buffer using DynaMag-2 Spin Magnet

(Thermo Fisher). Kinase assay performed on immunoprecipitated VPS34 using Class III PI3K ELISA Kit (K-3000, Echelon) through the protocol recommended for beads conjugated to enzyme. Kinase assay and PI3P production was performed at 30 °C for 1 h at 1100 r.p.m. Solution-containing PI3P was isolated from the magnetic beads using DynaMag-2 Spin Magnet and used for colorimetric detection of PI3P on ELISA plates.

Generation of NeuroMab *Inpp4b* antibody

Hybridoma cells that secrete NeuroMab clone N171/17-anti-INPP4b antibody were cultured in DMEM (Gibco) supplemented with 10% FBS (Gibco) and 1% penicillin-streptomycin (Gibco). Cells were passaged every 2 days up until 7 days before collection of antibody containing media by centrifugation at 200g. The antibody-containing media was directly applied to nitrocellulose membrane for *Inpp4b* detection.

Western blot

Whole cell lysates were generated using 1× RIPA buffer supplemented with protease inhibitor. Proteins were immunoblotted with the antibodies anti-LC3B (#3868), beta actin (#4967), INPP4B (#14543), LAMP1 (#3243) from Cell Signaling, anti-vATPase V1H (sc-166227), and cathepsin B (sc-365558) from Santa Cruz. Immunoblotting and immunoprecipitation of VPS34 was performed using the following antibody: Rabbit monoclonal antibody for PI3 Kinase Class III (1:1000 for Western blot or 1:50 for immunoprecipitation, 4263, Cell Signaling). Representative western blots used for figure generation are listed for visualization (Fig. S9).

Flow cytometry

MEF cells were incubated with 10 $\mu\text{g}/\text{ml}$ DQ-BSA (Invitrogen) or 1 mg/ml LY (Thermo Fisher) for 1 h to 6 h at 37 °C, or LTR 1 μM for 30 min, or Magic red for 1 h. Alternatively, LAMP1-mCherry signal of U2OS cells are recorded through flow cytometry following apilimod treatment. Briefly, cells were washed twice with PBS at each time point and whole cell fluorescence was recorded with the Beckman Coulter Cytoflex flow cytometer (Beckman). A total of 10,000 events was counted per condition per sample using the fluorescein isothiocyanate channel for DQ-BSA and LY or phycoerythrin channel for LTR and LAMP1-mCherry and Magic red. Background signal was determined from nonlabeled cells at time 0.

PtdIns labeling with ³H-myo-inositol and HPLC-coupled flow scintillation

MEF cells were incubated for two 24 h cycles with inositol-free media (MP Biomedical), 10% dialyzed FBS (Gibco), 4 mM L-glutamine (Sigma Aldrich), 1× insulin-transferrin-selenium-ethanolamine (Gibco), 20 $\mu\text{Ci}/\text{ml}$ myo-[2-³H(N)] inositol (PerkinElmer) and indicated treatment conditions. Cells were washed twice with 1× PBS between each 24 h cycle. Lipid precipitation induced, followed by lipid deacylation, extraction, and PtdIns separation by HPLC (Agilent

EDITORS' PICK: PIKfyve inhibition in Inpp4b-deficient MEF

Technologies) through anion-exchange 4.6 × 250-mm column (Phenomenex) as previously mentioned (CH *et al.*, 2018). β -RAM 4 (LabLogic) and 1:2 ratio of eluate to scintillation fluid (LabLogic) was used to detect radiolabeled eluate, followed by analysis with Laura 4 software (Ho *et al.*, 2016).

Quantitative RT PCR

RNA isolation from MEF cells was performed through Qiagen RNeasy mini kit (Qiagen). Superscript IV Vilo cDNA synthesis kit (Thermo Fisher) was used to reverse transcribe equal amount of mRNA. The resulting cDNA was amplified through quantitative PCR using TaqMan Fast Advanced Master mix (Applied Biosystems) according to manufacturer instructions in presence of Taqman assays with QuantStudio 3 Real-Time PCR system (Thermo Fisher) controlled by QuantStudio Design and Analysis Software version 1.2 (Thermo Fisher). Taqman assays include Actb (Mm02619580_g1), CtsD (Mm00515586_m1), CtsB (Mm00514443_g1), Atp6v1h (Mm01224350_m1), Atp6v1d (Hs00211133_m1), Lamp1 (Mm01217068_g1), and Mcoln1 (Mm01211241_g1) and were performed in triplicates. Relative quantification ($\Delta\Delta C_t$ method) was used to determine gene expression normalized to Actb and vehicle-treated WT MEF.

Statistical analysis

All experiments are conducted independently at least three times. All error bars represent SD. Statistical analysis to compare significance between multiple conditions were performed by ANOVA and post hoc analyses were performed with multiple Student's *t* test with Bonferroni correction. *p* values less than 0.05 considered were statistically significant.

Data availability

Upon Request

Supporting information—This article contains supporting information.

Acknowledgments—We thank all the members of the Salmena lab for thoughtful discussions and constructive criticism. The following plasmids were obtained from Addgene (Cambridge, MA): mCherry-Lysosomes-20 was a gift from Michael Davidson (Addgene plasmid # 55073), pBABE-puro mCherry-EGFP-LC3B was a gift from Jayanta Debnath (Addgene plasmid # 22418), pEGFP-N1-TFEB was a gift from Shawn Ferguson (Addgene plasmid # 38119), and pLJC5-Tmem192-3xHA was a gift from David Sabatini (Addgene plasmid # 102930). This work was supported in part by funds from the Department of Pharmacology and Toxicology and Temerty Faculty of Medicine, University of Toronto and awards from Canada Foundation for Innovation (CFI-#33505); The Natural Sciences and Engineering Research Council of Canada (NSERC-RGPIN-2015-03984) and Cancer Research Society grant (PIN 24261).

Author contributions—G. T. S. conceptualization; G. T. S. data curation; G. T. S. formal analysis; G. T. S. and L. S. investigation; G. T. S. and L. S. project administration; G. T. S. methodology; G. T. S. validation; G. T. S. software; G. T. S. visualization; G. T. S., R. J. B.,

and L. S. writing—original draft; G. T. S., R. J. B., and L. S. writing—review and editing; C. A. W., E. M. M., J. V., R. J. B., and L. S. resources; L. S. supervision; L. S. funding acquisition.

Funding and additional information—L. S. is the recipient of a Tier II Canada Research Chair (CRC) and was supported through the Human Frontier Career Development Program (HFSP) Award. R. J. B. contributions to this work was funded by Natural Sciences and Engineering Council of Canada (Discovery Grant RGPIN-2020-04343), the Canada Research Chairs Program (950-232333), and contributions from Ryerson University. This work was supported in part by funds from CIHR (MOP# 123343) awarded to J. V.

Conflict of interests—The authors declare no competing or financial interests.

Abbreviations—The abbreviations used are: FBS, fetal bovine serum; IF, immunofluorescence; INPP4B, inositol polyphosphate 4-phosphatase type II; LY, Lucifer yellow; MEF, mouse embryonic fibroblast; PIKfyve, Phosphoinositide Kinase, FYVE-Type Zinc Finger Containing; PtdIns(3)P, phosphatidylinositol-3-monophosphate; PtdIns(3,5)P₂, phosphatidylinositol-3,5-bisphosphate; PtdIns, phosphoinositide; TFEB, Transcription Factor EB.

References

1. Luzio, J. P., Rous, B. A., Bright, N. A., Pryor, P. R., Mullock, B. M., and Piper, R. C. (2000) Lysosome-endosome fusion and lysosome biogenesis. *J. Cell Sci.* **113**, 1515–1524
2. Settembre, C., and Ballabio, A. (2014) Lysosome: regulator of lipid degradation pathways. *Trends Cell Biol.* **24**, 743–750
3. Savini, M., Zhao, Q., and Wang, M. C. (2019) Lysosomes: signaling hubs for metabolic sensing and longevity. *Trends Cell Biol.* **29**, 876–887
4. Lamming, D. W., and Bar-Peled, L. (2019) Lysosome: the metabolic signaling hub. *Traffic* **20**, 27–38
5. Inpanathan, S., and Botelho, R. J. (2019) The lysosome signaling platform: adapting with the times. *Front. Cell Dev. Biol.* **7**, 113
6. Ebner, M., Koch, P. A., and Haucke, V. (2019) Phosphoinositides in the control of lysosome function and homeostasis. *Biochem. Soc. Trans.* **47**, 1173–1185
7. Dyson, J. M., Fedele, C. G., Davies, E. M., Becanovic, J., and Mitchell, C. A. (2012) Phosphoinositide phosphatases: just as important as the kinases. *Subcell. Biochem.* **58**, 215–279
8. Sasaki, T., Takasuga, S., Sasaki, J., Kofuji, S., Eguchi, S., Yamazaki, M., *et al.* (2009) Mammalian phosphoinositide kinases and phosphatases. *Prog. Lipid Res.* **48**, 307–343
9. McCartney, A. J., Zhang, Y., and Weisman, L. S. (2014) Phosphatidylinositol 3,5-bisphosphate: low abundance, high significance. *Bioessays* **36**, 52–64
10. Sbrissa, D., Ikononov, O. C., and Shisheva, A. (1999) PIKfyve, a mammalian ortholog of yeast Fab1p lipid kinase, synthesizes 5-phosphoinositides. Effect of insulin. *J. Biol. Chem.* **274**, 21589–21597
11. Bissig, C., Hurbain, I., Raposo, G., and van Niel, G. (2017) PIKfyve activity regulates reformation of terminal storage lysosomes from endolysosomes. *Traffic* **18**, 747–757
12. Sharma, G., Guardia, C. M., Roy, A., Vassilev, A., Saric, A., Griner, L. N., *et al.* (2019) A family of PIKfyve inhibitors with therapeutic potential against autophagy-dependent cancer cells disrupt multiple events in lysosome homeostasis. *Autophagy* **15**, 1694–1718
13. Dayam, R. M., Saric, A., Shilliday, R. E., and Botelho, R. J. (2015) The phosphoinositide-gated lysosomal Ca²⁺ channel, TRPML1, is required for phagosome maturation. *Traffic* **16**, 1010–1026
14. Mironova, Y. A., Lenk, G. M., Lin, J.-P., Lee, S. J., Twiss, J. L., Vaccari, I., *et al.* (2016) PI(3,5)P₂ biosynthesis regulates oligodendrocyte differentiation by intrinsic and extrinsic mechanisms. *Elife* **5**, e13023

15. Ho, C. Y., Alghamdi, T. A., and Botelho, R. J. (2012) Phosphatidylinositol-3,5-bisphosphate: no longer the poor PIP2. *Traffic* **13**, 1–8
16. Saffi, G. T., Tang, E., Mamand, S., Inpanathan, S., Fountain, A., Salmena, L., *et al.* (2021) Reactive oxygen species prevent lysosome coalescence during PIKfyve inhibition. *PLoS One* **16**, e0259313
17. Choy, C. H., Saffi, G., Gray, M. A., Wallace, C., Dayam, R. M., Ou, Z.-Y. A., *et al.* (2018) Lysosome enlargement during inhibition of the lipid kinase PIKfyve proceeds through lysosome coalescence. *J. Cell Sci.* **131**, jcs213587
18. Gayle, S., Landrette, S., Beeharry, N., Conrad, C., Hernandez, M., Beckett, P., *et al.* (2017) Identification of apilimod as a first-in-class PIKfyve kinase inhibitor for treatment of B-cell non-Hodgkin lymphoma. *Blood* **129**, 1768–1778
19. Bright, N. A., Gratian, M. J., and Luzio, J. P. (2005) Endocytic delivery to lysosomes mediated by concurrent fusion and kissing events in living cells. *Curr. Biol.* **15**, 360–365
20. Duclos, S., Corsini, R., and Desjardins, M. (2003) Remodeling of endosomes during lysosome biogenesis involves “kiss and run” fusion events regulated by rab5. *J. Cell Sci.* **116**, 907–918
21. Saffi, G. T., and Botelho, R. J. (2019) Lysosome fission: planning for an exit. *Trends Cell Biol.* **29**, 635–646
22. Hong, Z., Pedersen, N. M., Wang, L., Torgersen, M. L., Stenmark, H., and Raiborg, C. (2017) PtdIns3P controls mTORC1 signaling through lysosomal positioning. *J. Cell Biol.* **216**, 4217–4233
23. Law, F., Seo, J. H., Wang, Z., DeLeon, J. L., Bolis, Y., Brown, A., *et al.* (2017) The VPS34 PI3K negatively regulates RAB-5 during endosome maturation. *J. Cell Sci.* **130**, 2007–2017
24. Giridharan, S. S. P., Luo, G., Rivero-Rios, P., Steinfeld, N., Tronchere, H., Singla, A., *et al.* (2022) Lipid kinases VPS34 and PIKfyve coordinate a phosphoinositide cascade to regulate retriever-mediated recycling on endosomes. *Elife* **11**, e69709
25. Munson, M. J., Allen, G. F., Toth, R., Campbell, D. G., Lucocq, J. M., and Ganley, I. G. (2015) mTOR activates the VPS34-UVRAG complex to regulate autolysosomal tubulation and cell survival. *EMBO J.* **34**, 2272–2290
26. Jeschke, A., and Haas, A. (2018) Sequential actions of phosphatidylinositol phosphates regulate phagosome-lysosome fusion. *Mol. Biol. Cell* **29**, 452–465
27. Marat, A. L., Wallroth, A., Lo, W.-T., Müller, R., Norata, G. D., Falasca, M., *et al.* (2017) mTORC1 activity repression by late endosomal phosphatidylinositol 3,4-bisphosphate. *Science* **356**, 968–972
28. Rodgers, S. J., Ooms, L. M., Oorschot, V. M. J., Schittenhelm, R. B., Nguyen, E. V., Hamila, S. A., *et al.* (2021) INPP4B promotes PI3K α -dependent late endosome formation and Wnt/ β -catenin signaling in breast cancer. *Nat. Commun.* **12**, 3140
29. [preprint] Woolley, J. F., Chen, K., Genc, G. E., Lee, D. K. C., Dzneladze, I., He, R., *et al.* (2021) INPP4B promotes leukemia by restricting leukemic stem cell differentiation through regulation of lysosomal functions. *BioRxiv*. <https://doi.org/10.1101/2021.03.25.437029>
30. Baluska, F., Samaj, J., Hlavacka, A., Kendrick-Jones, J., and Volkmann, D. (2004) Actin-dependent fluid-phase endocytosis in inner cortex cells of maize root apices. *J. Exp. Bot.* **55**, 463–473
31. Chaurra, A., Gutzman, B. M., Taylor, E., Ackroyd, P. C., and Christensen, K. A. (2011) Lucifer Yellow as a live cell fluorescent probe for imaging water transport in subcellular organelles. *Appl. Spectrosc.* **65**, 20–25
32. Marwaha, R., and Sharma, M. (2017) DQ-red BSA trafficking assay in cultured cells to assess cargo delivery to lysosomes. *Bio Protoc.* **7**, e2571
33. Gray, M. A., Choy, C. H., Dayam, R. M., Ospina-Escobar, E., Somerville, A., Xiao, X., *et al.* (2016) Phagocytosis enhances lysosomal and bactericidal properties by activating the transcription factor TFEB. *Curr. Biol.* **26**, 1955–1964
34. Zhang, Y., McCartney, A. J., Zolov, S. N., Ferguson, C. J., Meisler, M. H., Sutton, M. A., *et al.* (2012) Modulation of synaptic function by VAC14, a protein that regulates the phosphoinositides PI(3,5)P₂ and PI(5)P. *EMBO J.* **31**, 3442–3456
35. [preprint] Saffi, G. T., Tang, E., Fountain, A., and Botelho, R. J. (2019) Reactive oxygen species rescue lysosome coalescence during PIKfyve inhibition. *BioRxiv*. <https://doi.org/10.1101/705491>
36. Sardiello, M., Palmieri, M., di Ronza, A., Medina, D. L., Valenza, M., Gennarino, V. A., *et al.* (2009) A gene network regulating lysosomal biogenesis and function. *Science* **325**, 473–477
37. Bright, N. A., Davis, L. J., and Luzio, J. P. (2016) Endolysosomes are the principal intracellular sites of acid hydrolase activity. *Curr. Biol.* **26**, 2233–2245
38. de Campos, C. B., Zhu, Y. X., Sepetov, N., Romanov, S., Bruins, L. A., Shi, C.-X., *et al.* (2020) Identification of PIKfyve kinase as a target in multiple myeloma. *Haematologica* **105**, 1641–1649
39. Runwal, G., Stamatakou, E., Siddiqi, F. H., Puri, C., Zhu, Y., and Rubinsztein, D. C. (2019) LC3-positive structures are prominent in autophagy-deficient cells. *Sci. Rep.* **9**, 10147
40. Klionsky, D. J., Abdelmohsen, K., Abe, A., Abedin, M. J., Abeliovich, H., Acevedo Arozena, A., *et al.* (2016) Guidelines for the use and interpretation of assays for monitoring autophagy (3rd edition). *Autophagy* **12**, 1–222
41. Zhang, X., Chen, S., Huang, K., and Le, W. (2013) Why should autophagic flux be assessed? *Acta Pharmacol. Sin.* **34**, 595–599
42. N'Diaye, E.-N., Kajihara, K. K., Hsieh, I., Morisaki, H., Debnath, J., and Brown, E. J. (2009) PLIC proteins or ubiquilins regulate autophagy-dependent cell survival during nutrient starvation. *EMBO Rep.* **10**, 173–179
43. Hansen, T. E., and Johansen, T. (2011) Following autophagy step by step. *BMC Biol.* **9**, 39
44. Kim, S., Choi, S., and Kang, D. (2020) Quantitative and qualitative analysis of autophagy flux using imaging. *BMB Rep.* **53**, 241–247
45. Ikonomov, O. C., Sbrissa, D., Venkatareddy, M., Tisdale, E., Garg, P., and Shisheva, A. (2015) Class III PI 3-kinase is the main source of PtdIns3P substrate and membrane recruitment signal for PIKfyve constitutive function in podocyte endomembrane homeostasis. *Biochim. Biophys. Acta* **1853**, 1240–1250
46. Bago, R., Malik, N., Munson, M. J., Prescott, A. R., Davies, P., Sommer, E., *et al.* (2014) Characterization of VPS34-IN1, a selective inhibitor of Vps34, reveals that the phosphatidylinositol 3-phosphate-binding SGK3 protein kinase is a downstream target of class III phosphoinositide 3-kinase. *Biochem. J.* **463**, 413–427
47. Korolchuk, V. I., Saiki, S., Lichtenberg, M., Siddiqi, F. H., Roberts, E. A., Imarisio, S., *et al.* (2011) Lysosomal positioning coordinates cellular nutrient responses. *Nat. Cell Biol.* **13**, 453–460
48. [preprint] Giridharan, S. S. P., Luo, G. S., Rivero-Rios, P. S., Steinfeld, N. S., Tronchere, H., Singla, A., *et al.* (2021) Lipid kinases VPS34 and PIKfyve coordinate a phosphoinositide cascade to regulate Retriever-mediated recycling on endosomes. *BioRxiv*. <https://doi.org/10.1101/2021.05.25.445615>
49. Liu, H., Paddock, M. N., Wang, H., Murphy, C. J., Geck, R. C., Navarro, A. J., *et al.* (2020) The INPP4B tumor suppressor modulates EGFR trafficking and promotes triple-negative breast cancer. *Cancer Discov.* **10**, 1226–1239
50. Zhang, J., Wang, J., Zhou, Z., Park, J.-E., Wang, L., Wu, S., *et al.* (2018) Importance of TFEB acetylation in control of its transcriptional activity and lysosomal function in response to histone deacetylase inhibitors. *Autophagy* **14**, 1043–1059
51. Brijmohan, A. S., Batchu, S. N., Majumder, S., Alghamdi, T. A., Thieme, K., McGaugh, S., *et al.* (2018) HDAC6 inhibition promotes transcription factor EB activation and is protective in experimental kidney disease. *Front. Pharmacol.* **9**, 34
52. Zhu, S.-Y., Yao, R.-Q., Li, Y.-X., Zhao, P.-Y., Ren, C., Du, X.-H., *et al.* (2021) The role and regulatory mechanism of transcription factor EB in health and diseases. *Front. Cell Dev. Biol.* **9**, 667750
53. Qiao, Y., Choi, J. E., Tien, J. C., Simko, S. A., Rajendiran, T., Vo, J. N., *et al.* (2021) Autophagy inhibition by targeting pikfyve potentiates response to immune checkpoint blockade in prostate cancer. *Nat. Cancer* **2**, 978–993
54. Martin, S., Harper, C. B., May, L. M., Coulson, E. J., Meunier, F. A., and Osborne, S. L. (2013) Inhibition of PIKfyve by YM-201636 dysregulates autophagy and leads to apoptosis-independent neuronal cell death. *PLoS One* **8**, e60152
55. Hessvik, N. P., Øverbye, A., Brech, A., Torgersen, M. L., Jakobsen, I. S., Sandvig, K., *et al.* (2016) PIKfyve inhibition increases exosome release and induces secretory autophagy. *Cell Mol. Life Sci.* **73**, 4717–4737
56. Sbrissa, D., Naisan, G., Ikonomov, O. C., and Shisheva, A. (2018) Apilimod, a candidate anticancer therapeutic, arrests not only PtdIns(3,5)P₂ but also PtdIns5P synthesis by PIKfyve and induces bafilomycin A1-reversible aberrant endomembrane dilation. *PLoS One* **13**, e0204532

EDITORS' PICK: *PIKfyve inhibition in Inpp4b-deficient MEF*



Golam T. Saffi is a postdoctoral researcher in the Department of Pharmacology & Toxicology at the Temerty Faculty of Medicine, University of Toronto. His research focuses on understanding phosphoinositide signaling and other cellular pathways that control lysosome functions and the implications of these functions in cell biology and disease. This study identifies a novel signaling axis between the catalytic functions of Inpp4b-PIKfyve-VPS34 in regulating lysosome morphology and dynamics.